Analytical Ion Thruster Discharge Performance Model

Dan M. Goebel*, Richard E. Wirz†, and Ira Katz‡
Jet Propulsion Laboratory, California Institute of Technology, Pasadena, CA 91109

A particle and energy balance model of the plasma discharge in magnetic ring-cusp ion thrusters has been developed. The model follows the original work of Brophy in the development of global 0-D discharge models that utilize conservation of particles into and out of the thruster and conservation of energy into the discharge and out of the plasma in the form of charged particles to the walls and beam and plasma radiation. The present model is significantly expanded over Brophy's original work by including self-consistent calculations of the internal neutral pressure, electron temperature, primary electron density, electrostatic ion confinement (due to the ring-cusp fields), plasma potential, discharge stability, and time dependent behavior during recycling. The model only requires information on the thruster geometry, ion optics performance and electrical inputs such as discharge voltage and currents, etc. to produce accurate performance curves of discharge loss versus mass utilization efficiency. The model has been benchmarked against the NEXIS Laboratory Model (LM) and Development Model (DM) thrusters, and successfully predicts the thruster discharge loss as a function of mass utilization efficiency for a variety of thrusters. The discharge performance model will be presented and results showing ion thruster performance and stability given.

Nomenclature

A	=	area	L	=	primary electron path length
A_a	=	plasma electron loss area	L_c	=	total cusp length
A_{as}	=	anode surface area	m	=	electron mass
A_p	=	primary electron loss area	M	=	ion mass
A_g	=	grid area	n_e	=	electron density
B	=	magnetic field strength	n_i	=	ion density
e	=	electron charge	n_o	=	neutral density
E	=	electric field in plasma edge	n_p	=	primary density
f_c	=	ion confinement factor	P	=	electron loss probability
I_a	=	ion current to the accelerator grid	P_o	=	neutral pressure
I_i	=	ion current	Q	=	neutral flow rate
I_{ia}	=	ion current to the anode	r_e	=	electron Larmor radius
I_e	=	cathode emission current	r_h	=	hybrid radius
I_B	=	beam current	r_i	=	ion Larmor radius
I_P	=	total ion production	r_p	=	primary Larmor radius
I_D	=	discharge current	T	=	effective grid transparency
I_K	=	ion current backflowing to cathode	T_e	=	electron temperature
I_L	=	primary current lost to anode	U^+	=	xenon ionization potential
I_s	=	ion current to the screen grid	U^*	=	xenon excitation potential
I^+	=	excited neutral production	v	=	velocity
Isp	=	specific impulse	v_e	=	electron velocity
k	=	Boltzman's constant	v_p	=	primary velocity
l	=	diffusion length	V_c	=	hollow cathode voltage drop

* Principal Scientist, Advanced Propulsion Group, Jet Propulsion Laboratory, Senior Member AIAA
† Senior Engineer, Advanced Propulsion Group, Jet Propulsion Laboratory, Member AIAA
‡ Group Supervisor, Advanced Propulsion Group, Jet Propulsion Laboratory, Member AIAA

V_D	=	discharge voltage	σ_+	=	excitation cross section
V_K	=	keeper voltage	σ	=	ion-neutral collision cross section
V_p	=	potential drop in plasma	ν_{en}	=	electron-neutral collision frequency
V	=	plasma volume	ν_{ei}	=	electron-ion collision frequency
ϕ	=	plasma potential relative to anode	ν	=	ratio of ν_{en} to ν_{ei}
η_c	=	Clausing factor	τ_c	=	primary collision time
η_D	=	discharge loss	τ_p	=	primary confinement time
η_m	=	mass utilization efficiency	τ_t	=	total thermalization time
σ_i	=	ionization cross section	μ_e	=	electron mobility

I. Introduction

Ion thrusters require efficient ionization of propellant atoms, which can be accomplished by a variety of plasma generation methods. These include DC electron discharges, rf and microwave discharges, and arc-plasma discharges. Ion thrusters that utilize electron discharges to produce the plasma, often called electron bombardment thrusters, have been flown on a NASA mission[1] and are now routinely used for station keeping on geosynchronous communications satellites[2]. Models of the discharge chamber performance in ion thrusters have been described in the literature for many years[3-6], but these models have been largely empirical and require detailed measurements of plasma parameters or thruster performance. Brophy developed the first comprehensive discharge chamber model[7] in the 1980's for ring-cusp magnetic confinement, electron bombardment thrusters based on particle and energy balance in the discharge chamber. This model assumed a uniform plasma and used volume averaged ionization and excitation rates, and has been called a 0-D or "single-cell' model. Brophy's model required some measurements of parameters in the thruster or data from plasma and gas flow simulations to accurately predict the thruster behavior. An improved version of this model was developed[8] with plasma potential and discharge stability effects[9], and was used to predict the performance of the NEXIS thruster[10,11]. This model still also required some plasma parameter inputs (such as electron temperature), and so was not a completely predictive tool.

Based on this previous work, a completely self-consistent analytical plasma discharge model has been developed for ring-cusp ion thrusters. The model requires only the mechanical configuration, the grid transparency from an ion optic code, the hollow cathode voltage drop, and electrical inputs to the discharge chamber to self consistently calculate the neutral gas pressure, electron temperature, primary density, ion and electron confinement, and plasma potential required to produce curves of discharge loss as a function of mass utilization efficiency. In addition, the model determines the plasma discharge stability for the discharge chamber size and magnetic field configuration, and explains the discharge behavior observed during recycling and turn on. These features make the 0-D ion thruster discharge chamber model predictive, which aides in the understanding of the discharge chamber performance for different thruster configurations. The 0-D model naturally does not address spatial non-uniformities, and so is best applied to fairly uniform plasma thrusters. However, the model still works well for hollow cathode discharges where the electrons from the localized electron source apparently disperse in the largely collisionless plasma and neutral density and the system is dominated by the average volume effects. The fully self-consistent model will be described and examples of its results presented.

II. Ion Thruster Design

Ion thrusters with a DC electron discharge plasma generator utilize a hollow cathode electron source and an anode potential discharge chamber that utilizes magnetic multipole boundaries to improve the ionization efficiency and generate the plasma from which ions are extracted by grids to accelerate the xenon ions to produce thrust at high specific impulse (Isp) to form the thrust beam. An illustration of an electron bombardment ion thruster is shown in Fig. 1. The four major components of the thruster are apparent: 1. discharge hollow cathode; 2. discharge chamber; 3, accelerator electrodes; and 4. neutralizer hollow cathode.

Electrons extracted from the hollow cathode enter the discharge chamber and ionize the injected propellant gas. Ions from this plasma flow to the accelerator structure and form the beam. Magnetic fields applied in the discharge chamber provide confinement primarily of the energetic electrons, which increase the electron path length prior to being lost to the anode wall and improves the ionization efficiency. The ion thruster schematic in Figure 1 shows an example of a ring-cusp thruster design with alternating magnetization rings of permanent magnets positioned around the thruster axis that produce a multi-pole magnetic field for plasma confinement. Proper design of the magnetic

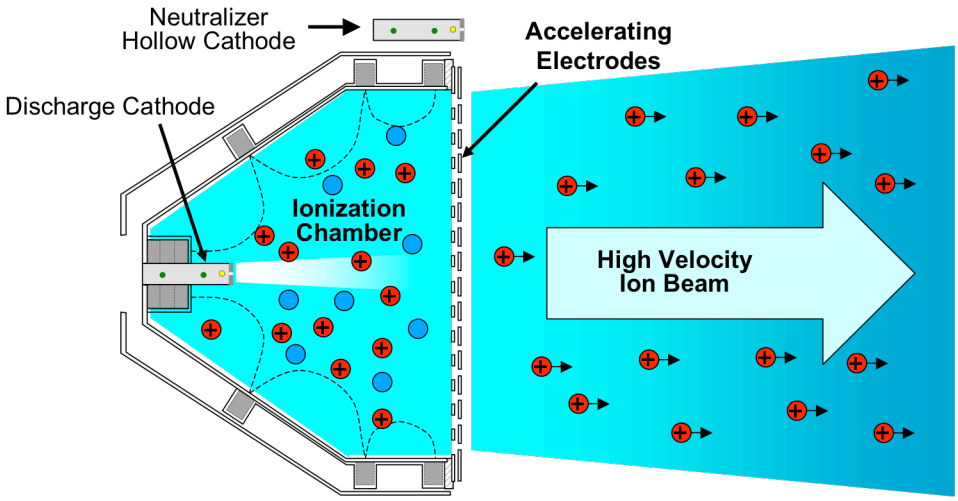

Figure.1. Illustration of an electron bombardment ion thruster.

field is critical to providing sufficient confinement to improve efficiency and adequate electron loss to produce stable discharges over the operation range of the thruster. Either two or three electrically biased grids at the thruster exit accelerate the ions to form the thrust beam. These grids will be described in the next section. Finally, a hollow cathode electron emitter is positioned outside the thruster body to provide electrons to neutralize the ion beam and maintain the potential of the thruster and spacecraft relative to the space plasma potential.

Several power supplies are required to operate the cathodes, electron discharge and accelerator in ion thrusters. A simplified electrical schematic typically used for ion thrusters is shown in Figure 2. The cathode heater and keeper supplies are not shown in this figure. The discharge supply is connected between the hollow cathode and the anode, and is normally run in the current regulated mode in order to provide stable discharges from the hollow cathode. The first grid, called the screen electrode, is normally connected to cathode potential in order to provide some confinement of the electrons in the discharge. Ions that penetrate the apertures in this grid are accelerated by the potential applied between the screen grid and the second grid, called the accelerator (or accel) grid. The high voltage bias is connected between the anode and the common of the system, which is normally connected to the neutralizer cathode and called neutralizer common. Positive ions born in the discharge chamber at high positive voltage are then accelerated out of the thruster. The accel grid is biased negative relative to the neutralizer common to prevent the very mobile electrons in the beam plasma from back-streaming into the thruster and overloading the screen supply. The ion beam is both charge and density neutralized by electrons from the neutralizer cathode, which self-biases the neutralizer common potential sufficiently negative relative to the space potential to produce the required number of electrons to neutralize the beam.

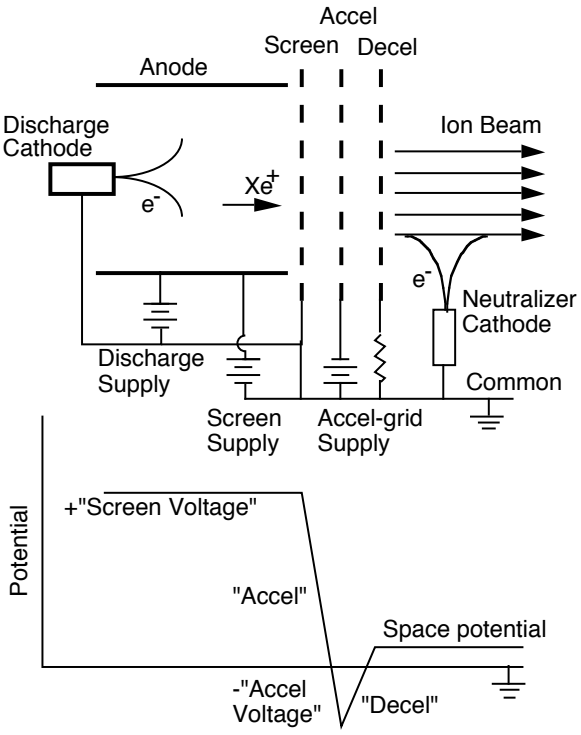

Figure 2. Electrical schematic of the ion thruster without the cathode heater and keeper supplies.

Figure 1 shows a three grid system, where a final grid called the “decel grid” is placed downstream of the accel grid. This grid shields the accel grid from ion bombardment from charge-exchanged produced ions in the beam backflowing toward the thruster, and eliminates downstream “pits and groves erosion” observed in two-grid systems. Three grid systems

therefore have longer accel grid life than two grid systems, and also generate less sputtered material into the plume that can impact the spacecraft.

Empirical studies over the past 50 years have investigated the optimal design of the magnetic field to confine the electrons and ions in thrusters. At this time, only two of these magnetic field geometries are still used in ion thrusters: the multipole magnetic field ring-cusp thrusters and the divergent solenoidal magnetic fields in Kaufman-type thrusters. Ring-cups thrusters use alternating polarity permanent magnet rings oriented perpendicular to the thruster axis, and the number of rings optimized for different size thrusters[8]. These thrusters provide magnetic confinement of the electrons with finite loss at the magnetic cusps, and electrostatic confinement of the ions from the anode wall due to the quasi-ambipolar potentials at the boundary caused by the transverse magnetic field. Line-cusp thrusters use a similar geometry but the cusps run axially along the chamber wall. Asymmetries at the ends of the line cusps cause plasma losses and difficulties in producing a uniform symmetric field at the cathode exit, which adversely affects the electron confinement and thruster efficiency.

III. 0-D Ion Thruster Model

The complete particle flows in a thruster discharge chamber are shown in Figure 3. The primary electron current emitted by the hollow cathode, Ie, generates ions and plasma electrons. The ions flow to the accelerator structure (I_s), to the anode wall (I_{ia}) and back to the cathode (I_k). Some fraction of the primary electrons are lost directly to the anode at the magnetic cusp (I_L). The plasma electrons are also lost to the anode at the cusp (I_a), with only a very small fraction lost transverse to the magnetic field between the cusps corresponding to the ambipolar current flows in this region.

The particle energies are determined by the potential distribution in the thruster. Figure 3 also schematically shows the potential in the plasma chamber. Electrons from the plasma inside the hollow cathode are extracted through the orifice and into the discharge chamber where they gain the energy $V_k = V_d - V_c + V_p + \phi$. Some of these electrons cause ionization near the hollow cathode output, which produces a higher plasma density locally near the cathode exit that must be dispersed before reaching the grid region in order to produce a uniform plasma profile across the grids. The potential drop in the plasma V_p can be approximated by $T_e/2$ due to the required pre-sheath potential to obtain the Bohm velocity. Electrons in the tail of the Maxwelian distribution overcome the anode sheath and are collected by the anode at the cusps.

A more complete model of the discharge chamber performance in ring-cusp thrusters than was covered in the previous section was developed by Brophy[7] in 1984. In his model, volume averaged particle and energy balance equations including primary electrons were used to derive expressions for the discharge loss as a function of the mass utilization efficiency in the thruster. Brophy's model was extended by Goebel[8] to include electrostatic ion confinement, primary confinement and thermalization, the anode sheath[9] and hollow cathode effects. This model utilizes magnetic field parameters obtained from a magnetic field solver that accurately models the magnetic boundary. Since the model assumes a relatively uniform plasma in the volume inside the magnetic multipole confinement at the surface of the discharge chamber, it is sometimes called a 0-D or "single-cell" model.

The upgraded 0-D model self-consistently calculates the neutral gas density, electron temperature, the primary electron density, plasma density, plasma potential, discharge current and the ion fluxes to the

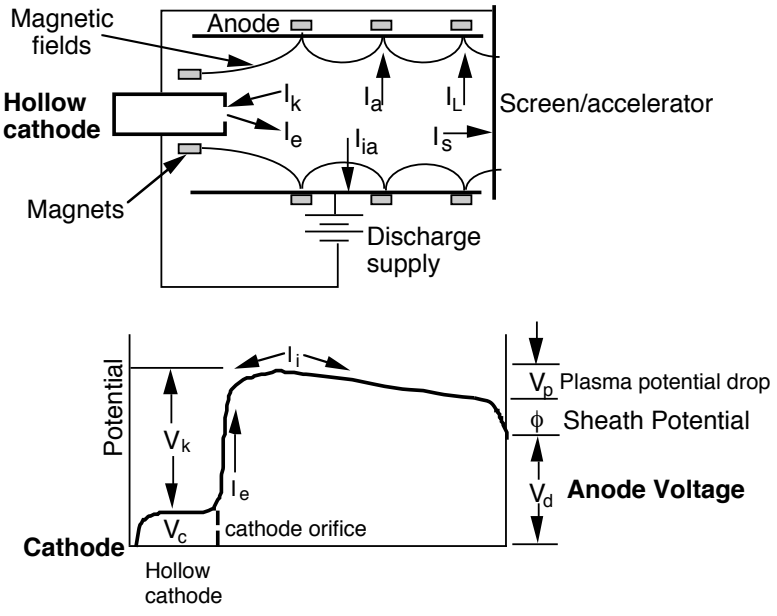

Figure 3. Schematic of thruster showing particle flows and potential distribution in the discharge chamber.

boundaries of the discharge chamber. While the assumption of a nearly uniform plasma is not particularly realistic near the cathode plume, the majority of the plasma in the discharge chamber is relatively uniform and the model predictions will be shown to be in excellent agreement with experimental results. The 0-D model then outputs discharge loss as a function of the mass utilization efficiency, which is useful in plotting performance curves that best characterize the discharge chamber performance.

The 0-D model is constructed as follows. The particle flows and potential distribution in the thruster were shown schematically in Figure 3. Mono-energetic primary electrons with a current I_e are assumed emitted from the hollow cathode orifice into the discharge chamber, where they ionize the background gas to produce a fairly uniform plasma. Electrons produced in the ionization process and thermalized primaries create a Maxwellian plasma electron population. Due to the relatively high magnetic field produced by the magnets near the wall, the electron Larmor radius is much smaller than the dimensions of the discharge chamber and the primary and plasma electrons are only lost at the magnetic cusp where the magnetic field lines are essentially perpendicular to the surface. Ions produced in the discharge chamber can flow back to the hollow cathode, to the anode wall or to the plane of the accelerator. At the accelerator, these ions are either intercepted and collected by the screen electrode with an effective transparency T, or enter the grids to become beam ions. The screen grid transparency depends on the optical transparency of the grid and the penetration of the high voltage fields from the accelerator region into the screen apertures. This transparency is calculated by ion optics codes, and is an input to the discharge model.

In this model, the high voltage power supply that accelerates the ions, called the screen supply, is connected to the anode. This means that the ions fall from the average plasma potential in the discharge chamber in form the beam. It is also possible to connect the screen supply to the screen and cathode, which means that the ion current in the beam must pass through the discharge supply. This changes the algebra slightly in calculating the discharge performance, but not the results. The components of particle and energy balance model are as follows.

A. Ion and Excited Neutral Production Rates

Ions are produced by both the primary electrons and by the tail of the Maxwellian distribution of the plasma electrons. The total number of ions produced in the discharge is given by

$$I_p = n_o n_e \langle \sigma_i v_e \rangle V + n_o n_p \langle \sigma_i v_p \rangle V, \tag{1}$$

where n_0 is the neutral atom density, n_e is the plasma electron density, σ_I is the ionization cross section, v_e is the plasma electron velocity, V is the plasma volume inside the discharge chamber, n_p is the primary electron density, and v_p is the primary electron velocity. The term in the brackets is ionization cross section is averaged over the distribution of electron energies, which is normally called the reaction rate coefficient.

An example of ionization cross sections commonly used for electrons impacting on xenon is shown in Figure 4. If it is assumed that the primary electrons are monoenergetic, then the reaction rate coefficient in Eq.1 for primary ionization is just the cross section in Fig. 4 times the corresponding primary electron velocity. If the primaries have a distribution in energy, then the cross section must be averaged over the distribution.

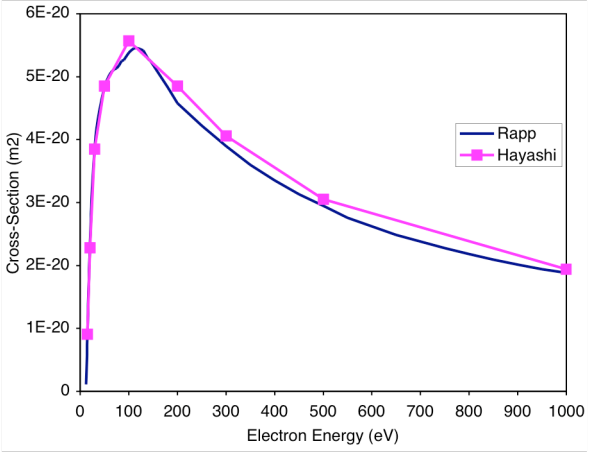

Figure 4. Ionization cross sections for xenon from Rapp and Hayashi

Excited neutrals are also produced by both the primary electrons and the tail of the Maxwellian distribution of the plasma electrons. The total number of exited neutrals produced in the discharge is given by

$$I^* = n_o n_e \langle \sigma^* v_e \rangle V + n_o n_p \langle \sigma^* v_p \rangle V, \tag{2}$$

where σ^* is the excitation cross section. Again, the excitation cross section is averaged over the distribution in electron energies to produce the reaction rate coefficients in the brackets. The reaction rate coefficients calculated by averaging the ionization and excitation cross sections over the Maxwellian energy distribution a shown in Figure 5. We see that the rate of excitation exceeds that of ionization if the electron temperature low (below about 8 eV). As can be seen in Fig. 5, at low electron temperatures a significant amount of the energy in the discharge goes into excitation of the neutrals at the expense of ionization. This is one of the (many) reasons that the cost of producing an ion in ion thrusters usually over ten times the ionization potential.

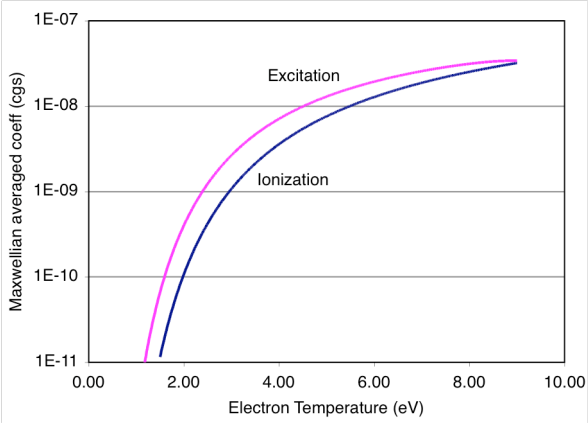

Figure 5. Ionization and excitation reaction rates for xenon from Rapp and Hayashi.

B. Electron Confinement at the Anode

The primary electrons injected into the discharge chamber from the hollow cathode bounce around the chamber volume until they are either lost directly to the anode wall by finding a cusp, make an ionization or excitation collision, or are thermalized by Coulomb interactions with the plasma electrons. The primary current to the anode cusps is given by

$$I_L = n_p v_p A_p \,, \tag{3}$$

where n_p is the primary electron density, v_p is the primary electron velocity, and A_p is the loss area for the primaries.

The loss area for primary electrons at the cusp is given by

$$A_p = 2\, r_p\, L_c = \frac{2}{B}\sqrt{\frac{2mv_p}{e}}\, L_c, \tag{4}$$

where r_p is the primary electron Larmor radius, B is the magnetic field strength at the cusp at the anode wall, v_p is the primary electron velocity, e is the electron charge, and L_c is the total length of the magnetic cusps (sum of the length of the cusps).

The primary electron confinement time is then

$$\tau_p = \frac{V}{v_p\, A_p} \,, \tag{5}$$

where V is the volume of the discharge chamber. The mean primary electron path length prior to finding a cusp and being lost to the wall is $L = v_p * \tau_p$. Likewise, the ionization mean free path is $\lambda = 1/n_o\sigma$, where σ represents the total inelastic collision cross section for the primary electrons. The probability that a primary electron will be lost to the anode is then

$$P = \left[1 - \exp^{-n_o \sigma L}\right] = \left[1 - \exp^{\left(-n_o \sigma V/A_p\right)}\right]. \tag{6}$$

By providing strong magnetic field strengths at the cusp to minimize the primary loss area, the probability of a primary electron being lost directly to the anode can be made very small. Likewise, ion thrusters with large volumes operated at higher internal gas densities will also reduce primary electron loss to the anode. Minimizing the energy loss associated with primaries being lost before making a collision in this way is required to maximize the efficiency of the thruster.

An example of the probability of a primary making a collision before finding a cusp is shown in Figure 6 for the case of the NEXIS thruster[10,11] designed with either 4 or 6 cusps. For the design with 6 cusps, it is required to have

cusp field strengths approaching 2000 G at the surface of the anode in order to ensure that the primaries are not lost prematurely. Designs with a smaller number of ring cusps, corresponding to a smaller primary anode collection area, require less magnetic field strength to achieve the same benefit. However, we will see later that the number of cusps affects efficiency and uniformity, and that maximizing the probability of a primary making a collision before being lost in Eq. 4.3.4-4 is only one of the trade-offs in designing an ion thruster.

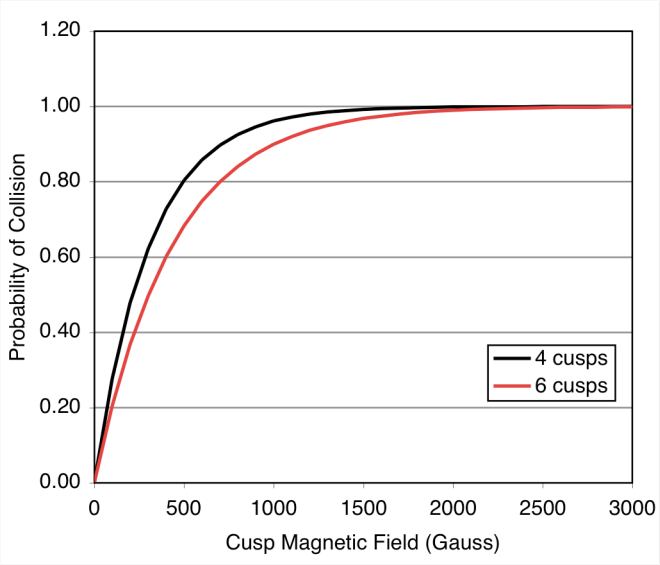

Figure 6. Probability of primary electrons making a collision before being lost to the anode as a function of magnetic field stength at the cusps.

Since the primary electron current lost directly to the anode is designed to be small for best efficiency, and the ion current is a small fraction of the discharge current, the discharge current is carried to the anode mainly by the plasma electrons. The plasma electrons are also only lost at the magnetic cusps, but their motions is affected by the ions penetrating the cusp and are lost to a hybrid anode area given by

$$A_a = 4\, r_h\, L_c = 4\sqrt{r_e r_i}\, L_c, \tag{7}$$

where r_h is the hybrid Larmor radius, r_e is the electron Larmor radius and r_i is the ion Larmor radius. The flux of plasma electrons I_a that overcomes the sheath at the anode is

$$I_a = \frac{1}{4}\left(\frac{8kT_e}{\pi m}\right)^{1/2} n_e A_a \exp^{-e\phi/kT_e}, \tag{8}$$

where ϕ is the plasma potential relative to the anode (essentially the anode sheath potential).

The plasma in the discharge chamber obeys particle conservation in that the current injected into the volume is the primary electron current, the current lost to the anode is the sum of the direct primary loss, the plasma electron loss and some ion loss, and the current lost to cathode potential surfaces and the accelerator is the ions that are produced in the discharge. The plasma potential will adjust itself such that the plasma electron current to the anode is equal to the ion current out of the discharge. For a given plasma density and temperature, which determines the random electron flux incident on the sheath, changing the anode area will change the sheath voltage, which affects both the energy loss though the sheath and the stability of the discharge.

C. Ion Confinement at the Anode

Ions are typically unmagnetized in ion thruster discharge chambers because the low applied magnetic field results in a large ion Larmor radius compared to the thruster dimensions. That implies that the flux of ions out the plasma volume in any direction is given by the Bohm current:

$$I_i = \frac{1}{2} n_i \sqrt{\frac{kT_e}{M}} A, \tag{9}$$

where n_i is the ion density in the center of the discharge and A is the total ion loss area. However, the magnetized electrons influence the ion motion by electrostatic effects, causing largely ambipolar flows to the walls. It is possible to analyze the electron and ion transport across the magnetic field between the cusps and calculate the reduction in the ion velocity caused by the reduced transverse electron drift speed. This can be used to calculate the rate of ion loss to the anode compared to the unmagnetized Bohm current ion loss rate (to the grids).

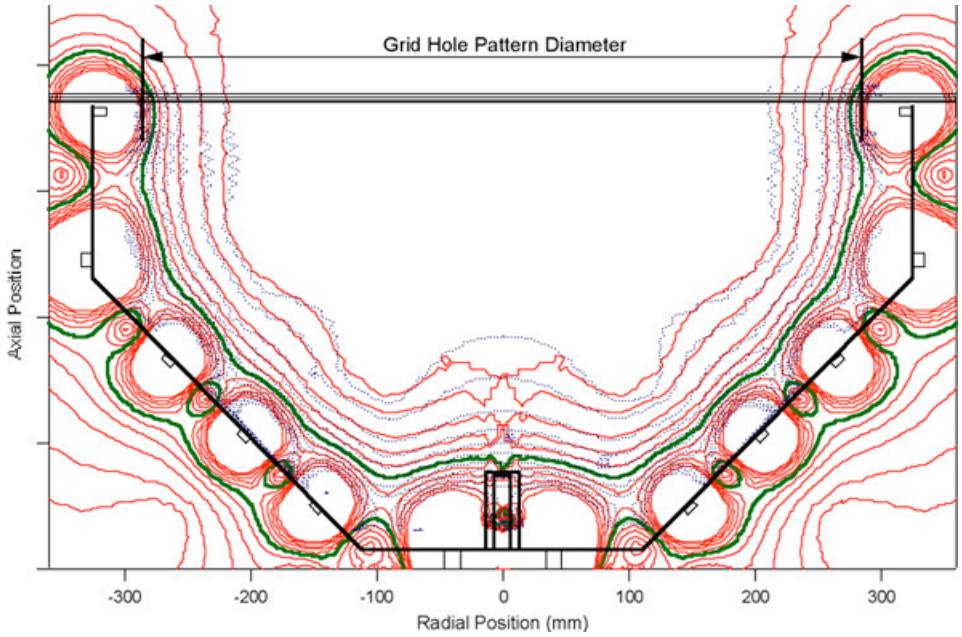

Figure 7. Example of measured and calculated magnetic field contours for a ring-cusp thruster discharge chamber[10] utilizing 6 rings of SmCo magnets.

Ring cusp thrusters can be designed with various numbers of rings, distances betweens the rings, and magnet sizes that determines the magnetic field strength in the discharge chamber. The magnetic multipole boundary in ring cusp structures produces radial and aximuthal components of the magnetic field. While analytical calculations of the field strength in the multipole structure are possible, it is much more common to utilize a commercial available 2-D or 3-D magnetic field solver, like the commercial Maxwell 3-D code[12], to find the fields. Figure 7 shows the measured and calculated contours of constant magnetic field strength for an example 6-ring cusp thruster design[10]. The 60-gauss contour is closed all along the boundary, which will be shown to provide good ion confinement between the cusps.

To evaluate the ion loss across the magnetic field, the steady state transverse electron equation of motion, including electron-neutral and electron-ion collisions, is given by

$$mn\left(\frac{dv_e}{dt} + (v \bullet \nabla)v\right) = -en(E + v_e x B) - kT\nabla n - mn\nu_{en}(v_e - v_o) - mn\nu_{ei}(v_e - v_i) = 0, \tag{10}$$

where v_o is the neutral velocity. This equation must be separated into the two transverse velocity components:

$$v_x + \mu_e E + \frac{e}{m\nu_e} v_y B + \frac{kT}{m\nu_e}\frac{\nabla n}{n} - \frac{\nu_{ei}}{\nu_e} v_i = 0 \tag{11}$$

$$v_y + \mu_e E - \frac{e}{m\nu_e} v_x B + \frac{kT}{m\nu_e}\frac{\nabla n}{n} - \frac{\nu_{ei}}{\nu_e} v_i = 0 \tag{12}$$

where $\nu_e = \nu_{en}+\nu_{ei}$, $\mu_e = e/m\nu_e$, and we neglect v_o compared to v_e. Solving for v_y and eliminating the ExB and diagmagnetic drift terms in the v_x direction, the transverse electron velocity is given by

$$v_e\left(1 + \mu_e^2 B^2\right) = \mu\left(E + \frac{kT}{e}\frac{\nabla n}{n}\right) + \frac{\nu_{ei}}{\nu_e} v_i \ . \tag{13}$$

Assuming ambipolar diffusion, we equate the electron and ion transverse velocities to give

$$v_i = \frac{\mu_e}{\left(1+\mu_e{}^2B^2 - \frac{\nu_{ei}}{\nu_e}\right)}\left(E + \frac{kT}{e}\frac{\nabla n}{n}\right). \tag{14}$$

This can be written in terms the transverse electron flux as

$$J_\perp = \frac{\mu_e}{\left(1+\mu_e{}^2B^2 - \frac{\nu_{ei}}{\nu_e}\right)}\left(enE + kT\nabla n\right), \tag{15}$$

The minimum magnetic field to produce an ion velocity v_i is given by

$$B = \frac{\nu_e m_e}{e}\sqrt{\frac{e}{m_e \nu_e v_i}\left(E + \frac{T_e}{\ell}\right) - \left(\frac{\nu}{1+\nu}\right)}, \tag{16}$$

where $\nu=\nu_{en}/\nu_{ei}$, and $\nabla p/en=\nabla(nkT_e)/en$ is approximately T_e/l for l representing the length the ions travel radially in the transverse magnetic field between the cusps. The value of l can be estimated from calculations of the transverse magnetic field versus the distance from the wall between the cusps, and is usually on the order of 2 to 3 cm. Setting E=0 in Eq. 16 gives the case of $v_i = v_{thermal}$, which essentially cancels out the pre-sheath potential that normally accelerates the ions to the Bohm velocity with the ambipolar electric field from the reduced transverse-mobility electrons. The flux of ions passing through the transverse magnetic field is then reduced, and this smaller ion flux is finally accelerated to the Bohm velocity close to the anode wall to satisfy the sheath criterion.

However, it is not necessary to limit this to the case of E=0. If the magnetic field is smaller than the critical B that causes E=0, then the transverse electron mobility increases and a finite electric field exists in the magnetic width l. The ions fall through whatever potential difference is set up by this electric field, which means that the ions are accelerated to an energy given by

$$\frac{1}{2}mv_i^2 = eE_{total} \bullet l. \tag{17}$$

The transverse magnetic field and ambipolar flow change the electric field magnitude in the presheath region and reduces the acceleration of the ions toward the wall. However, in the limit of no magnetic field, the electric field must accelerate the ions only to the Bohm velocity, which results in a net electric field in the plasma edge-region given by

$$E = -\frac{mv_i^2}{e\,l}. \tag{18}$$

Note that the electric field sign must be negative because we are accelerating ions outward. The minimum magnetic field is then

$$B = \frac{\nu_e m_e}{e}\sqrt{\frac{e}{m_e \nu_e v_i}\left(\frac{T_e}{\ell} - \frac{mv_i^2}{\ell}\right) - \left(\frac{\nu}{1+\nu}\right)}, \tag{19}$$

which can be solved for the ion velocity v_i versus B.

The parameters in the terms $\nu_e = \nu_{en}+\nu_{ei}$ and $\nu=\nu_{en}/\nu_{ei}$ are given in SI units[13] for xenon as:

$$\nu_{en} = \sigma\sqrt{\frac{8eT_e}{\pi m}}, \quad \sigma = 6.6\text{x}10^{-19}\left(\frac{T_e}{4} - 0.1\Big/\left(1+\frac{T_e}{4}\right)^{1.6}\right),$$
$$\nu_{ei} = 2.9\text{x}10^{-12}\,\frac{n_e \ln\Lambda}{T_e^{3/2}}, \qquad \ln\Lambda = 23 - 0.5\ln\left(\frac{10^{-6}n_e}{T_e^3}\right) \tag{20}$$

where lnΛ is the Coulomb logarithm. Since we know that the Bohm velocity is $\sqrt{T_e/M}$, it is a simple matter to calculate the value of B for a given ratio of the ion velocity v_I to the Bohm velocity. If we define a confinement factor $f_c = v_i/v_{Bohm}$, the ion current transverse to the magnetic field between the cusps to the anode is given by

$$I_{ia} = \frac{1}{2} n_i \sqrt{\frac{kT_e}{M}} A_{sa} f_c , \tag{21}$$

where A_{sa} is the surface area of the anode exposed to the plasma.

For the case of the NSTAR ion thruster, the fraction of the Bohm current to the anode (I_{ia}/I_{Bohm}) is shown in Figure 8. We see that at zero transverse magnetic field, the ion flux to the anode is just the Bohm current. As the transverse field reduces the electron mobility, the ions are slowed. In the NSTAR design[14], the last close magnetic contour is about 20 Gauss, and so 50% of the ions initially headed radially toward the anode are lost. For closed magnetic field contours of about 50 Gauss, the ion loss to the anode is reduced by nearly a factor of ten compared to the unmagnetized Bohm current. This can make a significant difference in the efficiency of the plasma generator and amount of discharge power required to produce the beam ions. We see that even though the ions are unmagnetized, ambipolar effects make the cusp magnetic fields very effective in reducing the ion loss to the walls.

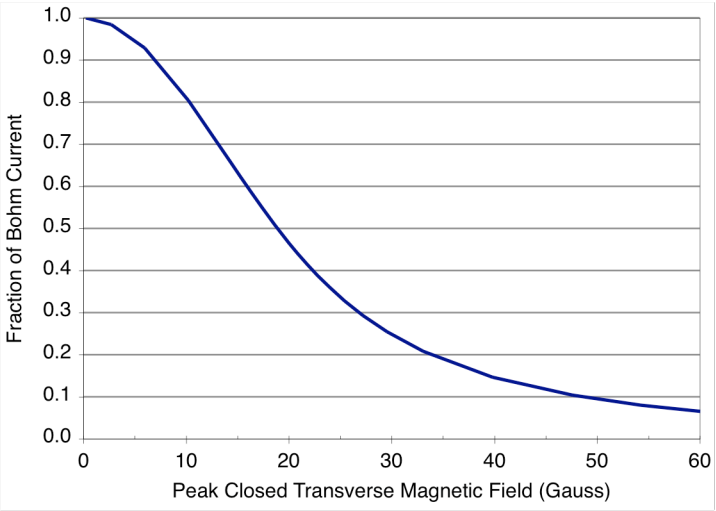

Figure 8. Fraction of the Bohm current density to the anode wall as a function of the peak transverse magnetic field.

D. Plasma and Neutral Parameters in the Discharge Chamber

The ion and excited neutral production rates described by Eqs. 1 and 2 contain the neutral gas density in the discharge chamber. The neutral gas that escapes the chamber (the unionized propellant) is the gas injected into the discharge chamber minus the gas particles that are ionized and form the beam:

$$Q_{out} = Q_{in} - I_B . \tag{22}$$

The neutral gas that leaks through the grid is the neutral flux on the grids times the grid optical transparency T and a conductance reduction term called the Clausing factor:

$$Q_{out} = \frac{1}{4} n_o v_o A_g T \eta_c , \tag{23}$$

where v_o is the neutral gas velocity, A_g is the grid area and η_c is the Clausing factor. The Clausing factor represents the reduced conductance of the grids for finite grid thicknesses. For typical grid apertures with small thickness to length ratios, the Clausing factor must be calculated using Monte Carlo techniques. In general, ion thruster grids will have Clausing factors on the order of 0.5.

The mass utilization efficiency of the thruster is defined as

$$\eta_m = \frac{I_B}{Q_{in}} \ . \tag{24}$$

Equating 22 and 23 and solving for the neutral gas density in the discharge chamber gives

$$n_o = \frac{4Q_{in}(1-\eta_m)}{v_o A_g T \eta_c} = \frac{4\, I_B}{v_o A_g T \eta_c} \frac{(1-\eta_m)}{\eta_m} . \tag{25}$$

The neutral pressure in the discharge chamber, P_o, during operation of the thruster can be found using this expression and the conversion:

$$P_o\,[\text{Torr}] \ = \ 1.04\text{x}10^{-25}\ n_o\left[\frac{\text{particles}}{m^3}\right] * T_o[\text{K}]. \tag{26}$$

where T_o is the neutral gas temperature in the discharge chamber.

The electron temperature in the discharge chamber can be calculated from particle balance of the ions. The total ion production rate, given by Eq. 1, must equal the total ion loss rate. The ion loss rate can be considered to be the Bohm current in Eq. 3 with the area A representing the sum of all the surfaces A_i that collect ions (cathode, anode and grids). Equating 22 and 23, and using Eq. 24 gives

$$\frac{\sqrt{\frac{kT_e}{M}}}{\langle \sigma_i v_e \rangle V + \frac{n_p}{n_e}\langle \sigma_i v_p \rangle V} = \frac{2n_o V}{A_i} = \frac{8\ V\ I_B}{v_o A_g A_i T \eta_c} \frac{(1-\eta_m)}{\eta_m} . \tag{27}$$

If the beam current is specified (and therefore the average plasma density n_e) and the primary electron density calculated, this equation can be solved for the electron temperature, which is a variable in the ion and electron velocities. Typically, curve fits to the ionization and excitation cross section and reaction rate data shown in Figs. 5 and 6 are used to evaluate the reaction rate coefficients in a program that iterative solves Eq. 27 for the electron temperature.

The primary electron density in Eq. 27 can be evaluated from the primary electron confinement times in the discharge chamber. The emitted current I_e from the hollow cathode is

$$I_e = \frac{n_p V}{\tau_t} , \tag{28}$$

where τ_t is the total primary confinement time. The ballistic confinement time for direct primary loss to the anode, τ_p, was given in Eq. 5. It is assumed that primaries that have undergone an inelastic collision with the neutral gas has lost sufficient energy such that it is then rapidly thermalized with the plasma electrons. The mean time for a collision between the primary and a neutral gas atom to occur is given by

$$\tau_c = \frac{1}{n_o \sigma v_p} . \tag{29}$$

Using Eq. 25 for the neutral density, the mean collision time is

$$\tau_c = \frac{v_o A_g T \eta_c}{4\ \sigma v_p I_B} \frac{(1-\eta_m)}{\eta_m} . \tag{30}$$

The total primary electron confinement time can be found from

$$\frac{1}{\tau_t} = \frac{1}{\tau_p} + \frac{1}{\tau_c} \ . \tag{31}$$

The current emitted from the hollow cathode is

$$I_e = I_d - I_{sc} - I_k \ . \tag{32}$$

Using Eq. 30 and 31, the primary electron density is given by

$$n_p = \frac{I_e \, \tau_t}{V} = \frac{I_e}{V}\left[\frac{1}{\tau_p} + \frac{1}{\tau_c}\right]^{-1} = \frac{I_e}{V}\left[\frac{v_p A_p}{V} + \frac{4\sigma v_p I_B (1 - \eta_m)}{v_o A_s T \eta_c \eta_m}\right]^{-1} . \tag{33}$$

If we assume that the primary electron loss directly to the anode is negligible and the ion current back to the cathode is small, then Eq. 33 becomes

$$n_p = \frac{I_e v_o A_s T \eta_c \eta_m}{4V\sigma v_p I_B} \frac{\eta_m}{(1 - \eta_m)} = \frac{(I_d - I_{sc}) v_o A_s T \eta_c \eta_m}{4V\sigma v_p I_B} \frac{\eta_m}{(1 - \eta_m)} \ . \tag{34}$$

This equation demonstrates the characteristic behavior originally described by Brophy[7] of the primary electron density being proportional to the mass utilization efficiency divided by one minus the mass utilization efficiency. The dependence is valid unless there are other energy-loss paths for the primary electrons such as thermalization with the plasma electrons.

E. Power and Energy Balance

The power into the discharge chamber is the emitted current from the hollow cathode times the energy of the electrons going into the discharge. If we neglect the potential drop in the plasma (which is only about $T_e/2$ for our uniform plasma assumption), the input power is

$$P_{in} = I_e(V_d - V_c + \phi), \tag{35}$$

where V_d is the discharge voltage and ϕ is the plasma potential in the discharge chamber relative to the anode wall. The power into the discharge goes into producing ions, excited neutrals and Maxwellian electrons. The power from the discharge to the electrodes is from by ions flowing to the anode, cathode and screen plane, and from primary and plasma electrons flowing to the anode. The power out of the discharge is then given by:

$$P_{out} = I_p U^+ + I^* U^* + I_s(V_d + \phi) + I_k(V_d + \phi) + I_B\phi + I_{ia}\phi + I_a(2T_e + \phi) + I_L(V_d - V_c + \phi), \tag{36}$$

where I_p is the total number of ions produced in the discharge, U^+ is the ionization potential of the propellant gas, I^* is the number of excited ions produced in the discharge chamber, U^* is the excitation energy, I_s is the number of ions to the screen plane, I_k is the number of ions flowing back to the cathode, I_B is the beam current, I_a is the plasma electron current to the anode, T_e is the electron temperature, I_{ia} is the ion current to the anode, and I_L is the primary electron fraction lost to the anode. The plasma electron energy lost to the anode wall, given as $2T_e+\phi$ in Eq. 36, is calculated in Reference X.

Since the screen grid is usually connected to the cathode potential, conservation of particles gives

$$I_e = I_d - I_s - I_{ik} \quad \text{and} \quad I_a = I_d + I_{ia} - I_L \ , \tag{38}$$

where I_d is the discharge current measured in the discharge power supply. Equating the power into the discharge to the power out, using the particle balance equations in 4.3.6.3, and solving for the beam current from the thruster gives

$$I_B = \frac{I_d\left(V_d - V_c - 2T_e\right)}{\phi\left(I_p U^+ + I^* U^* + \left(I_s + I_k\right)\left(2V_d - V_c + 2\phi\right) + I_{ia}\left(2T_e + 2\phi\right) + I_L\left(V_d - V_c - 2T_e\right)\right)} \quad . \tag{39}$$

The issue in evaluating Eq. 39 for the beam current produced by a given thruster design is that several of the current terms in the denominator contain the plasma density, which is not known. In addition, the beam current I_B is given by the Bohm current averaged over the screen-grid plane times the effective transparency T of the grid:

$$I_B = \frac{1}{2} n_i v_a A_s T = \frac{1}{2} n_i \sqrt{\frac{kT_e}{M}} A_s T \approx \frac{1}{2} n_e \sqrt{\frac{kT_e}{M}} A_s T, \tag{40}$$

where n_i is the peak ion density at the screen grid, v_a is the ion acoustic velocity, A_s is the screen grid area, and T is the effective screen transparency with high voltage applied to the accelerator grids. In this equation, quasi-neutrality ($n_i \approx n_e$) is assumed. Equations 39 can be solved for the plasma density using Eqs. 40:

$$n_e = \frac{I_d\left(V_d - V_c - 2T_e\right)}{\frac{I_p}{n_e} U^+ + \frac{I^*}{n_e} U^* + \frac{(1-T) v_a A_s}{2}\left(2V_d - V_c + 2\phi\right) + \frac{v_a A_{sa} f_c}{2}\left(2T_e + 2\phi\right) + n_p v_p A_p\left(V_d - V_c - 2T_e\right)} \quad , \tag{41}$$

where the current intercepted by the screen grid, I_s, given by

$$I_s = \frac{(1-T)}{2} n_i v_a A_s = \frac{(1-T)}{2} n_i \sqrt{\frac{kT_e}{M}} A_s, \tag{42}$$

was used. Unfortunately, the ion and excitation currents in this equation (from Eqs. 1 and 2) still contain terms proportion to n_p/n_e, so Eq 42 must be solved parametrically for the plasma density. This can be accomplished with simple spreadsheet iterative programs. Once the plasma density is known, the beam current can be calculated from Eq. 40, and the peak plasma density obtained by dividing these results by the flatness parameter for the thruster obtained from probe measurements or 2-D codes of the discharge chamber.

F. Discharge Loss

The discharge loss in an ion thruster is defined as

$$\varepsilon_d = \frac{I_d V_d}{I_B} \quad , \tag{43}$$

Combining Eqs. 39 and 43, the discharge loss is

$$\varepsilon_d = \frac{V_d\left[\frac{I_p}{I_B} U^+ + \frac{I^*}{I_B} U^* + \frac{\left(I_s + I_k\right)}{I_B}\left(2V_d - V_c + 2\phi\right) + \phi + \frac{I_{ia}}{I_B}\left(2T_e + 2\phi\right) + \frac{I_L}{I_B}\left(V_d - V_c - 2T_e\right)\right]}{V_d - V_c - 2T_e} \quad . \tag{44}$$

We can now evaluate the current fractions in this equation. Ions are produced by both the primary electrons from the hollow cathode and by the tail of the Maxwellian distribution of the plasma electrons. The total number of ions produced in the discharge was given in Eq. 1, and the total number of excited neutrals produced in the discharge was given in Eq. 2. Using these equations and Eq. 40 for the beam curent, and assuming $n_i \approx n_e$, the first current fraction in Eq. 44 is

$$\frac{I_p}{I_B} = \frac{2n_o n_e \langle \sigma_i v_e \rangle V}{n_i \sqrt{\frac{kT_e}{M}} A_s T f_p} + \frac{2n_o n_p \langle \sigma_i v_p \rangle V}{n_i \sqrt{\frac{kT_e}{M}} A_s T} = \frac{2n_o V}{T \sqrt{\frac{kT_e}{M}} A_s} \left(\langle \sigma_i v_e \rangle + \frac{n_p}{n_e} \langle \sigma_i v_p \rangle \right), \tag{45}$$

and the second current fraction is likewise:

$$\frac{I^*}{I_B} = \frac{2n_o V}{T \sqrt{\frac{kT_e}{M}} A_s} \left(\langle \sigma_* v_e \rangle + \frac{n_p}{n_e} \langle \sigma_* v_p \rangle \right). \tag{46}$$

Neglecting the ion current backflowing to the cathode as small, the third current fraction is

$$\frac{I_s}{I_B} = \frac{1 - T}{T}. \tag{47}$$

The ion current that goes to the anode wall is again the Bohm current reduced by the confinement factor f_c described above. In this theory, the confinement factor for ions to the anode is found from a current fit to the solution of Eq. 14 evaluated for the particular ion thruster discharge chamber being analyzed. In general for most ion thrusters, if the 50 Gauss contour is closed it is possible to assume to first order that $f_c \approx 0.1$ and the ion loss is essentially one tenth of the local Bohm current. The fourth current fraction in Eq. 4.3.9-2 is then

$$\frac{I_{ia}}{I_B} = \frac{\frac{1}{2} n_i \sqrt{\frac{kT_e}{M}} A_{sa} f_c}{\frac{1}{2} n_i \sqrt{\frac{kT_e}{M}} A_s T} = \frac{A_{sa} f_c}{T A_s}, \tag{48}$$

where A_{sa} is the surface area of the anode facing the plasma in the discharge chamber.

The primary electron current lost to the anode, I_L, is given by Eq. 3. The last current fraction in Eq. 44 is then

$$\frac{I_L}{I_B} = \frac{n_p v_p A_p}{\frac{1}{2} n_i v_a A_s T} = \frac{2 n_p v_p A_p}{n_e v_a A_s T}. \tag{49}$$

The discharge loss can then be written

$$\varepsilon_d = \frac{V_d \left[\frac{I_p}{I_B} U^+ + \frac{I^*}{I_B} U^* + \frac{1 - T}{T} (2V_d - V_c + 2\phi) + \phi + \frac{A_{as} f_c}{T A_s} (2T_e + 2\phi) + \frac{2 n_p v_p A_p}{T n_e v_a A_s} (V_d - V_c - 2T_e) \right]}{V_d - V_c - 2T_e}. \tag{50}$$

At first glance, it appears that the discharge loss increases directly with the discharge voltage. However, V_d appears in both the numerator and denominator in Eq. 50, so the direct dependence is weak and increases in V_d increase the primary energy strongly, which increases the ionization rate and beam current. Higher discharge voltages always result in lower discharge losses. Equation 50 illuminates the design features that improve the discharge efficiency. Higher screen grid transparency T, smaller ion confinement factor f_c (better ion confinement), smaller anode area A_a at the cusps all reduce the discharge loss. Lowering the plasma potential also will reduce the discharge loss by reducing the energy lost to the anode by the plasma electrons.

While Eq. 50 may appear complicated, it consists entirely of parameters that are either inputs to the discharge chamber design or operation, or parameters that can be easily calculated. The input data required to evaluate the discharge loss for a ring cusp thruster are

- Discharge voltage
- Discharge chamber surface area and volume

- Magnetic field design (magnetic field at the cusp and the closed contour field between the cusps)
- Grid area and effective transparency
- Neutral gas temperature in the discharge chamber
- Hollow cathode voltage drop

It is necessary to specify either the discharge current or the beam current in order to calculate the plasma density in the discharge chamber. The grid transparency is obtained from the grid codes (called "optics codes") such as the JPL CEX-2D ion optics code[15]. The cathode voltage drop is either measured inside the hollow cathode[16], or calculated using a separate 2-D hollow cathode plasma models[17].

Discharge chamber behavior is characterized by "performance curves", which are plots of discharge loss versus mass utilization efficiency. These curves provide the electrical cost of producing beam ions as a function of the propellant utilization efficiency, and give useful information of how well the plasma generator works. Performance curves are normally taken at constant beam current and discharge voltage so that the efficiency of producing and delivering ions to the beam is not masked by changes in the discharge voltage or average plasma density at the grids.

IV. Model Predictions

Calculating performance curves using Eq. 50 requires iteration of the solutions for the electron temperature, discharge current and/or beam current in the above equations. In practice, discharge current and total gas flow and gas flow split between the cathode and main discharge chamber are varied to produce a constant beam current and discharge voltage as the mass utilization efficiency changes. This means that a beam current and mass utilization operating point can be specified, which determines the neutral gas density in the discharge chamber from Eq. 25 and average plasma density in the discharge chamber from the Bohn current. If a discharge current is then specified, the primary electron density can be calculated from Eq. 34 and the electron temperature found from evaluating Eq. 27. These parameters are then used to solve for the discharge loss in Eq. 50. The discharge current is then evaluated from the given beam current, discharge voltage and discharge loss. The program is iterated until a discharge current is found that produces the correct discharge loss at the specified beam current.

An example of performance curves calculated using this model and compared to measured curves for the NEXIS thruster are shown in Figure 9. The discharge loss was measured for three different discharge voltages during operation at 4 A of beam current. We see that the model matches the measured the discharge loss well. The 180 eV/ion discharge loss at 26.5 V required that the thruster run at a discharge current of 27.8 A to produce the 4 A of ion beam current. The shape of the performance curves is important. At high mass utilization, the neutral density in the discharge chamber is low and more of the primary energy goes into the plasma electrons and direct loss to the anode. The higher electron temperature increases energy loss to the anode by the plasma electrons and increases the radiation losses by excitation at a fixed beam current. Optimal thruster designs will have flatter discharge performance curves in order to provide high mass utilization at reasonably low discharge losses.

An important requirement of discharge models for ion thrusters is to handle the primary electrons as correctly as possible. For the case described here of monoenergetic primaries, the primary density is determined by collisional and ballistic (direct-anode) losses that change as a function of the neutral pressure. If primary electron are neglected altogether (assumed thermalized immediately in the cathode plume) so that the plasma is produced only by ionization by the tail of the Maxwellian electron population, the discharge loss is extremely high. This is shown in Fig. 10, where the discharge loss increases to over 240 eV/ion if the primary electrons are neglected entirely. Likewise, if the primary electron density is assumed to

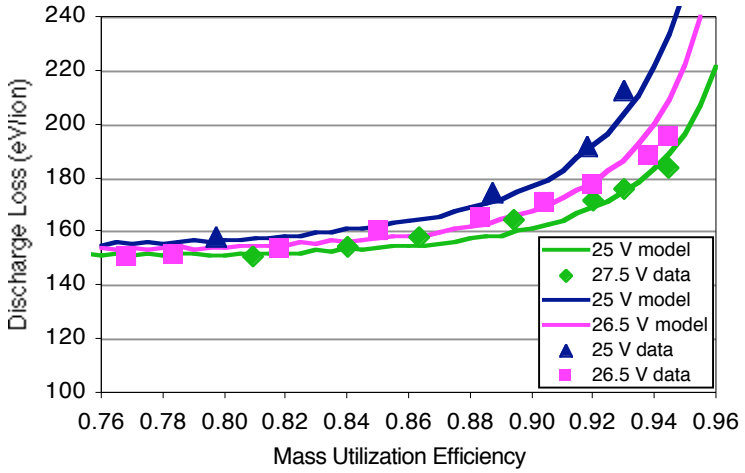

Figure 9. Example of the discharge loss versus mass utilization efficiency for three different discharge voltages in the NEXIS thruster, where the symbols represent the data and the solid curves represent the model predictions.

be constant and independent of the neutral pressure, then the discharge loss curve in Fig. 10 has a steep slope resulting from excessive primary ionization at high pressures (low mass utilization). Clearly, correct handing of the primary electron generation and loss rates is important. In reality, the primary electrons have a spread in energy and are better represented by a drifted Maxwellian distribution, which will not be covered in this paper.

Having a representative model of the discharge permits environmental changes to the thruster to be understood. For example, the neutral gas temperature depends on the operating time of the thruster until equilibrium is reached, which can take hours in some cases. The 0-D discharge chamber model accurately showed the change in discharge loss as the NEXIS thruster heated up after turn on based on the change in the neutral gas temperature[10].

The discharge model works very well on other thrusters. Figure 11 shows the NEXT thruster[18] discharge loss at various throttle points, and the model predictions for the NEXT geometry. Performance data for the full curve at 3.52 A (not shown) also agreed well with the model results. Similar good agreement has been obtained for the XIPS ion thruster.

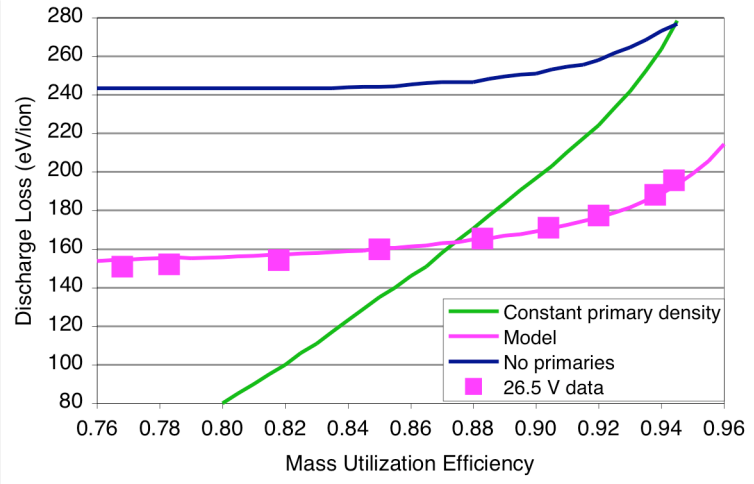

Figure 10. Discharge loss predictions for the cases of no primary electron density and a constant primary electron density showing the poor agreement with the measurements.

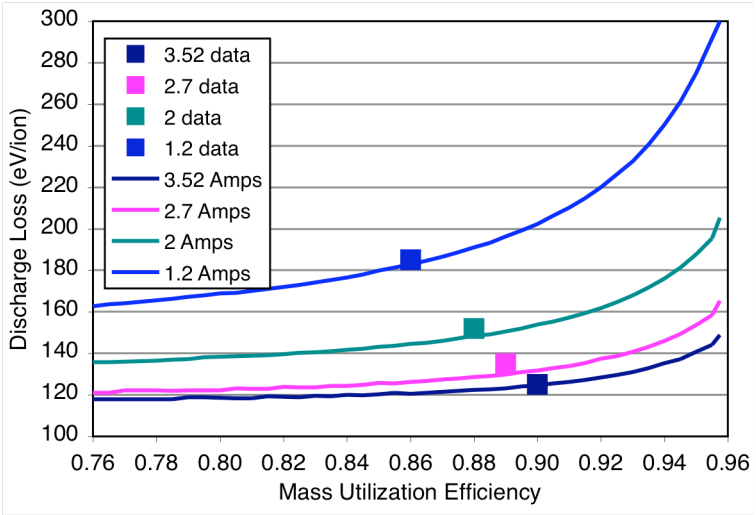

Figure 11. Discharge loss versus mass utilization efficiency for the NEXT thruster[18].

V. Discharge Stability

There is a strong relationship between the discharge loss and the stability of the discharge. We saw from inspection of Eq. 50 that the efficiency increases if the anode area for primary electrons is minimized. While it is logical to assume that this is also true if the anode area for plasma electrons is minimized to reduce the energy loss to the Maxwellian population, a dependence on A_a does not appear in Eq. 50. However, since the discharge current is carried primarily by the plasma electrons, the sheath potential at the anode given in Eq. 8 is found to decrease as the anode area for plasma electron decreases. The sheath potential dependence is seen in the discharge loss equation, which suggests that minimizing the sheath potential maximizes the efficiency. However, the anode area for plasma electrons cannot go to zero because the discharge current could not be collected by the anode and the discharge would either interrupt or go unstable. So there is a minimum anode area and plasma potential, which must be determined.

The value of the plasma potential relative to the anode (the anode sheath voltage drop) can be calculated using Eq. 8. The electron current to the anode at the cusp is found from Eq. 38:

$$I_a = I_d + I_{ia} - I_L. \tag{51}$$

Using Eqs. 3, 8, 21 and dividing by the beam current in Eq. 9, Eq. 51 becomes

$$\frac{I_d}{I_B}+\frac{\frac{1}{2}n_e v_a A_{as} f_c}{\frac{1}{2}n_e v_a A_s T}-\frac{n_p v_p A_p}{\frac{1}{2}n_e v_a A_s T}=\frac{\frac{1}{4}\left(\frac{8kT_e}{\pi m}\right)^{1/2} n_e A_a}{\frac{1}{2}n_e v_a A_s T}\exp^{-e\phi/kT_e}. \tag{52}$$

Solving for the plasma potential gives

$$\phi=\frac{kT_e}{e}\ln\left[\frac{\left(\frac{2M}{\pi m}\right)^{1/2}\frac{A_a}{A_s T}}{\frac{I_d}{I_B}+\frac{A_{as}f_c}{A_s T}-\frac{2n_p v_p A_p}{n_e v_a A_s T}}\right]. \tag{53}$$

As seen in Eq. 53, as the anode area decreases the plasma potential goes down. If the anode area is made too small, then the plasma potential will go negative relative to the anode potential. This is called a positive going (ore electron accelerating) anode sheath. In this case, the anode area available is insufficient to collect the total discharge current by collection the entire incident random electron flux on the cusp area. The plasma then biases itself to pull in electrons in the Maxwellian distribution not headed toward the anode, which delivers more current to satisfy the charge balance requirement. However, once the potential goes sufficiently negative relative to the anode to repel the ions (about T_i), then the anode area for the plasma electron is not the hybrid area, but just twice the plasma electron Larmor radius times the cusp length, similar to Eq. 4 for the primary loss area. This results in a significant decrease in the cusp anode area, further lowering the plasma potential relative to the anode. Examining the potential distribution in the plasma in Figure 3, we see that the positive-going anode sheath will subtract from the primary electron energy. The ionization rate then decreases, and the discharge collapses into a high impedance mode or oscillates between this mode and a positive potential typically on power supply time constants as the supply tries to reestablish the discharge by increasing the anode voltage.

The stability of the plasma discharge at a given operating point (discharge current, beam current, pressure, etc.) is therefore determined by the magnetic field design. For example, in Figure 12, the 0-D model predicts that a four-ring design of a strawman thruster would be unstable (when the potential goes negative relative to the anode) for cusp magnetic fields greater than 2000 G. Since strong magnetic fields are desirable from a primary electron and ion confinement point of view, additional rings are required to maintain a positive plasma potential. A six ring design increased the anode area sufficiently to raise the plasma potential at the 2000 G magnet design point. This came at some loss of efficiency, which appears to always be the trade off.

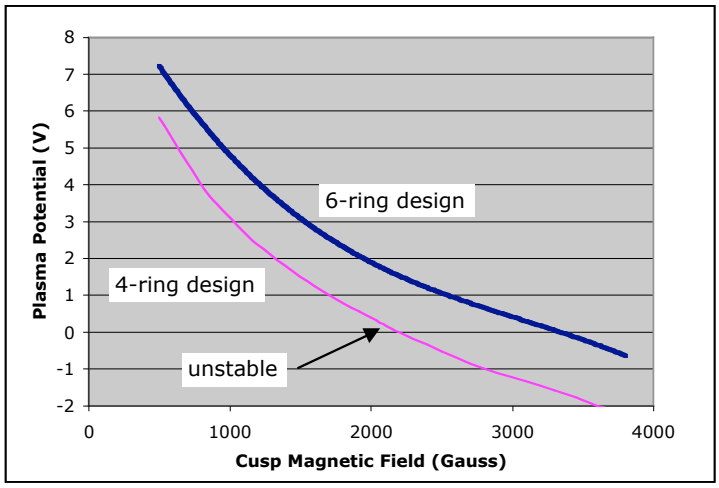

Figure 12. Plasma potential versus cusp magnetic field strength for a thruster design with 4 and 6 rings.

Finally, the 0-D model predicted the correct magnetic field design for stability at the desired operating point, but the discharge was found to go unstable (oscillate) during recycles. In a recycle, the high voltage is turned off momentarily in order to clear a high voltage breakdown somewhere in the thruster grids or body. Without high voltage on, ions that would have left the discharge chamber as beam ions now tend to strike the accelerator grid and back flow into the discharge chamber as neutrals. This raises the neutral gas pressure in the discharge chamber, which is seen in the calculated pressure with time in Fig. 13a. This has two effects. First, the higher neutral pressure then tends to collisionally thermalize the primary electrons more rapidly, which can lead to a reduction in the plasma potential[9], which is shown in Fig. 13 b where the plasma potential decreases in the discharge chamber as the pressure rises with time after the recycle starts. Second, it is standard to reduce the discharge current during the recycle to reduce the ion current bombarding the accel grid and make it easier to restart the engine by limiting the amount of positive charge in the grid gaps that the power supplies must sink to reestablish the high voltage. Lowering the discharge current while raising the neutral pressure leads to a lower impedance discharge and a lower discharge voltage. This effect also contributes reducing the plasma potential. Finally, the potential decreases below the anode voltage after sufficient time, as seen in Fig. 13c, and the discharge goes unstable. This instability occurs because the anode sheath has inverted (now positive going), which reflects the ions. Since the ions are no longer reaching the wall at the cusp, the anode area becomes the electron loss area instead of the hycrid loss area, which is much smaller. As seen from Eq. 53, the smaller anode area further decreases the plasma potential, and the plasma potential runs away negatively. This results in an oscillation because the primary energy decreases as the plasma potential decreases (see Fig. 3), and so the ionization also decreases. The lower density does not support the discharge current, and the power supply increases the voltage trying to obtain the discharge current. The system oscillates between these states until the pressure is reduced or the discharge voltage increased.[9] This situation is mitigated by increasing the anode area such that the discharge current can be carried by a lower density plasma.

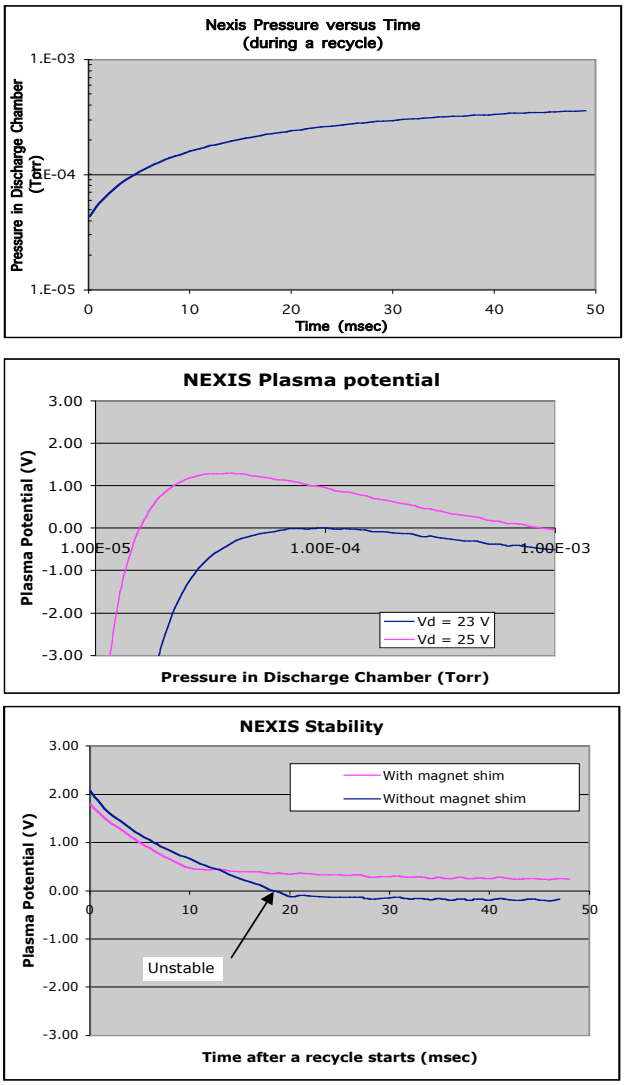

Figure 13c Pressure increase with time from a recycle (a), plasma potential as a function of pressure for two different magnet designs (b), and plasma potential versus time (c) showing instability of the smaller anode area design at a given pressure.

VI. Conclusion

The self-consistent discharge plasma model described here provides good agreement with the experimental data and a predictive capability for ion thruster performance. While 0-D models like this can provide very good information on the design parameters of thrusters and can predict their performance reasonably well, there are several limitations to their use. First, the model assumes a uniform neutral gas and plasma density and averages the ion production and loss throughout the volume of the discharge chamber. For ion thrusters with significantly non-uniform plasmas, such as NSTAR[14], this leads to inaccuracies especially at high mass utilization efficiencies where the double ion production is high on axis. In addition, since the source of the gas is from the localized hollow cathode aperture and the gas manifold inside the discharge chamber, the neutral density is also not uniform. These

issues, along with the problem of dispersing the cathode plume, have to be modeled by full 2-D discharge chamber codes such as developed by Wirz and Katz.[19] However, simple 0-D models such as this get you over "90% of the way there", and are very useful in understanding ion thruster performance and behavior.

Acknowledgments

The research described in this paper was carried out by the Jet Propulsion Laboratory, California Institute of Technology.

References

[1]J.R. Brophy, D. E. Brinza, J. Polk, M. Henry, A. Sengupta, "The DS1 Hyper-Extended Mission", AIAA Paper No. 2002-3673 (2002).

[2] D. M. Goebel, M. Martinez-Lavin, T. A. Bond, and A. M. King "Performance of XIPS Electric Propulsion in Station Keeping of the Boeing 702 Spacecraft", AIAA-2002-5117, 38th Joint Propulsion Conference, Indianapolis, IN (2002).

[3]H.R. Kaufman, "An Ion Rocket with an Electron-Bombardment Ion Source", NASA Technical Note, TN-D-585 (1961).

[4]T.D. Maske, "Plasma Properties and Performance of Mercury Ion Thrusters," AIAA Journal, **9**, p.205-212, (1971).

[5]J. Ward, T. Masek, "A discharge Computer Model for an Electron Bombardment Thruster", AIAA Paper No. 76-1009 (1976).

[6]J.N.Matossian, J.R. Beattie, "Model for Computing Volume Averaged Plasma Properties in Electron-Bambardment Ion Thrusters", J. Propulsion and Power, **5**, p.188-196 (1989).

[7]J.R. Brophy, Ion Thruster Performance Model", NASA CR-174810, Ph.D. Thesis, Colorado State University, Dec. 1984.

[8]D. M. Goebel, J.E. Polk, and A. Sengupta, "Discharge Chamber Performance of the NEXIS Ion Thruster", AIAA-2004-3813, 40th AIAA Joint Propulsion Conference, Fort Lauderdale, FL, July 11-14, 2004.

[9]D.M. Goebel "Ion Source Discharge Performance and Stability", Physics of Fluids, 25 (1982) 1093.

[10]J. Polk, D.M. Goebel, J.S.Snyder, A.C.Schneider, L.Johnson, A. Sengupta "Performance and Wear Test Restuls for a 20-kW-Class Ion Engine with Carbon-carbon Grids", AIAA-2005-4393, 41th AIAA Joint Propulsion Conference, Tucson, AZ, July 10-13, 2005.

[11]T. Randolph and J. Polk, "An Overview of the Nuclear Electric Xenon Ion System (NEXIS) Activity", AIAA-2004-3450, 40th AIAA Joint Propulsion Conference, Fort Lauderdale, FL, July 11-14, 2004.

[12]Maxwell 3-D is a product of Ansoft Corp., URL: http://www.ansoft.com/products/em/max3d/overview.cfm.

[13]Book, D. NRL Plasma Formulary, 1998.

[14]J.R. Brophy "NASA's Deep Space 1 Ion Engine", Rev. Sci.Instrum. **73** (2002) p.1071-1078

[15]J. J. Anderson, I. Katz and D. Goebel, "Numerical Simulation of Two-Grid Ion Optics Using a 3D Code", AIAA-2004-3782**,** 40th Joint Propulsion Conference, Ft. Lauderdale, FL July 2004.

[16]D.M.Goebel, K. Jameson, R. Watkins, I. Katz, "Cathode and Keeper Plasma Measurements Using an Ultra-Fast Miniature Scanning Probe" AIAA-2004-3430, 40th Joint Propulsion Conference, Ft. Lauderdale, FL July 2004.

[17]I. Mikellides, I. Katz, D.M.Goebel. and J. Polk, "Theoretical Model of a Hollow Cathode Insert Plasma," AIAA Paper 04-3817, July 2004.

[18]G.C.Soulas, M.T. Domonkos, M.J. Patterson, "Performance Evaluation of the NEXT Ion Engine", AIAA-2003-5278, 38th AIAA Joint Propulsion Conference, Huntsville, AL, July 20-23, 2003.

[19]R. Wirz and I. Katz, "Plasma Processes in DC Ion Thruster Discharge Chambers", AIAA-2005-3690, 41th AIAA Joint Propulsion Conference, Tucson, AZ, July 10-13, 2005.